Engineering Fracture Mechanics 77 (2010) 2749–2762

Contents lists available at ScienceDirect

Engineering Fracture Mechanics

journal homepage: www.elsevier.com/locate/engfracmech

Fracture surfaces and the associated failure mechanisms in ductile iron with different matrices and load bearing

Ricardo A. Martínez *

División Metalurgia – INTEMA – UNMDP – CONICET, J.B. Justo 4302, (7600) Mar del Plata, Pcia. de Buenos Aires, Argentina

ARTICLE INFO

Article history:
Received 29 December 2009
Accepted 19 July 2010
Available online 24 July 2010

Keywords:
Ductile iron
Matrix
Fracture surface
Mechanism
Load

ABSTRACT

Ductile iron (DI) is a family of cast alloys that covers a wide range of mechanical properties, depending on its matrix microstructure. For instance, ferritic matrices used in parts, such as automotive suspension components, demand high impact properties and ductility among some of their main requirements. On the other hand, pearlitic and martensitic matrices are used when hardness, strength and wear resistance are of particular concern. When it comes to very high strength parts, ausferritic matrices, typically austempered ductile iron (ADI), are widely used.

DI has been employed to replace cast and forged steels in a large number of applications and its production has shown a sustained rate of growth over the last decades.

Knowing about failure modes and fracture mechanisms associated to materials with the properties mentioned above is crucial, since they can be of great value for designers of mechanical components.

This paper deals with the analysis of fracture surfaces of ductile cast iron generated under different conditions of load application, temperature and environments.

The studies include the examination of fracture surfaces obtained by means of tensile tests, impact tests and by samples used to determine fracture toughness properties, where the zones of fatigue pre-crack and monotonic load condition were evaluated. A special case of ductile iron fracture is also examined.

The study of the different surfaces permitted to establish patterns that contributed to unveil the fracture mechanisms of ductile iron with different matrices, nodule count, etc.
© 2010 Elsevier Ltd. All rights reserved.

1. Introduction

Ductile iron (DI) production has reached a sustained growth rate over the last decades in the global market. To a certain extent, this can be attributed to the improvements achieved in molding, fusion and casting techniques as well as to the metallurgical advances attained, which have significantly enhanced mechanical properties [1].

Other advantages include the possibility of applying DI to different size parts and complex geometries, thereby providing effective manufacturing solutions to certain applications.

DI mechanical properties are basically defined by its microstructure, which is made up of free-graphite spheroids and a metallic matrix. The microconstituents present in the matrix vary depending on different parameters, such as their chemical composition, cooling rate after being poured in a mold, and solid state heat treatments.

Bearing in mind the parameters above mentioned, ferrite, pearlite, or mixes of both can be obtained under as cast conditions. By means of heat treatment, martensite, pearlite, ferrite or ausferrite (austempered ductile iron, ADI) can be attained using quenching, normalizing, annealing or austempering, respectively.

* Tel.: +54 2234816600; fax: +54 2234810046.
E-mail address: rimarti@fi.mdp.edu.ar

0013-7944/$ - see front matter © 2010 Elsevier Ltd. All rights reserved.
doi:10.1016/j.engfracmech.2010.07.013

Another aspect worth considering when it comes to analyzing the mechanical properties of ductile iron is its associated solidification process. A brief description could be the following: graphite and austenite nucleate independently into liquid, with the austenite growing dendritically. As the solidification process advances, the austenite dendrites trap the surrounding nodules. Carbon diffusion to the nodules makes them grow by diffusion in solid state. By so doing, one dendrite contains several nodules. Then the dendrites and nodules grow together into isolated liquid zones that solidify at the end of the process. These zones between dendrites are known as the last to freeze (LTF) zones. Given the fact that LTF zones solidify at the end of the process, the concentration of some alloy elements and impurities may diffuse and concentrate in these zones as well as in small shrinkage cavities [2,3].

Chemical elements such as Mg, C, Mn, Si, S, and P are always present in ductile cast irons, whereas, elements like Mo, Cu, and Ni are frequently found as alloy elements. It is worth noticing that the concentration of these elements in the metallic matrix is not homogeneous, but rather significantly irregular. This characteristic is known as *segregation*. Most chemical elements feature segregation properties, which occur during the solidification process. Two segregation levels can be distinguished: *microsegregation* and *macrosegregation,* the first is present in a range of approximately some hundreds of microns (μm). Macrosegregation, in turn, occurs in a greater range. Unlike macrosegregation, which can be effectively controlled, microsegregation cannot be avoided; it always occurs.

As a consequence, during the solidification process microsegregation promotes additional microstructural aspects between the bulk zones of the matrix and the LTF zones [4], which are common to all the matrices described earlier.

Hence, the DI fracture process should be analyzed on a material with hollow spherical bubbles of different sizes (the strength of the graphite occupying these sites is negligible), taking into account the metallic matrix (a great variety of microstructures are possible) and certain sites in the matrix (LTFs) where microporosity, cast defects, non-metallic inclusions (sand from molds) retained austenite, and carbides are present.

By analyzing the description above, it can be concluded that the fracture process would be different with a particular fracture mechanism in each case.

There are three main types of fractures in metals and alloys. The first one is related to ductile materials which usually fail as a result of nucleation, growth and coalescence of voids, and initiate at inclusions and second phase particles. The second one is cleavage, in which the fracture involves separation along specific crystallographic planes. In this case, the fracture path is transgranular. Even though cleavage is often called brittle fracture, it can be preceded by large scale plasticity and ductile crack growth. With respect to the third one, it is the intergranular fracture, which occurs when the grain boundaries are the preferred fracture path for cracks propagation in the material [5–7].

This work reports some experimental data derived from test samples using different types of loads (tensile, bending, and cyclic loads), load rates (slow monotonic and impact), and test temperatures in the case of impact samples.

The fracture micromechanisms were analyzed using SEM.

This research work is intended to provide a better understanding of DI complex fracture processes.

2. Experimental methods

Different ductile cast iron melts were prepared in a medium frequency induction furnace. Steel scrap and foundry returns were used as raw materials. Nodulization was carried out using the sandwich method, employing 1.5 wt% of Fe–Si–Mg (6% Mg).

One inch "Y" blocks were cast in sand molds. Round bars of 12 mm diameter were cut from the Y blocks and used to prepare metallographic and tensile test samples. The melts, with a pearlitic – ferritic matrix under as cast conditions, were heat treated to obtain the different matrices used in this study. The specific heat treatment (HT) applied is particularized in the caption of each set of microphotographs under discussion.

The chemical composition was determined by using a Baird DV6 spectrometer.

The examinations were conducted by means of scanning electron microscopy (SEM), using a JEOL model JSM-6460LV.

Microstructure characterization, nodule count, nodularity, nodule size and details of the matrix were characterized and described for each case of fracture surface under study, using conventional procedures of polishing and etching. Observations were made using an optical microscope Olympus PGM.

Cylindrical test specimens of ¼ in. (6.35 mm) diameter (ASTM E8M/88/04) for tensile tests, unnotched Charpy impact specimens of $10 \times 10 \times 55$ mm for impact tests (ASTM E23-02a), and SEN(B) specimens of $10 \times 20 \times 90$ for fracture toughness tests (ASTM E390-90) were machined from "Y" blocks (ASTM A536-84). Fig. 1 displays the specimens used.

Tensile and three-point bending tests were performed using a universal testing machine INSTRON model 8501, and the impact test using a pendulum AMSLER 130/688.

Crack propagation was induced by means of a displacement controlled cyclic load, using a mechanical testing machine with a double eccentric actuator.

A constant eccentricity of $e = 0.145$ mm was chosen for all tests. Stable crack propagation was attained following these conditions under small scale plasticity. The frequency of the cyclic load was of 6 Hz.

Taking advantage of a particular embrittlement phenomenon suffered by ADI, a special interrupted tensile test was carried out. The results of this work are accounted for in Section 3.

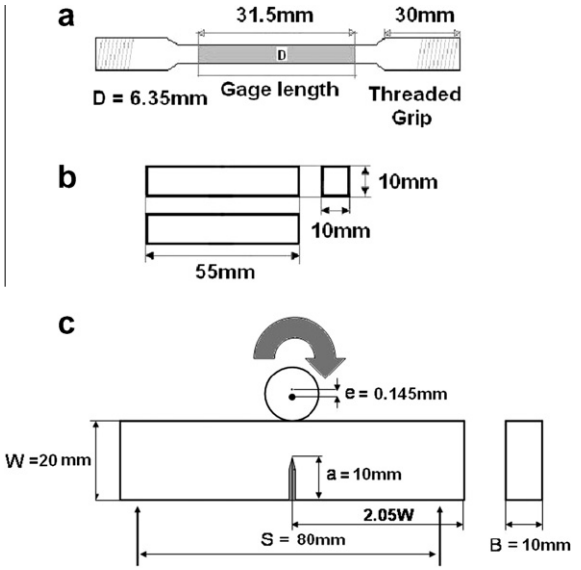

Fig. 1. Samples used for mechanical testing.

3. Results and discussion

The results reported in this paper derive mainly from fracture surface observations. A description of the surface and a proposed fracture mechanism are developed. Information such as the value of the measured mechanical property, chemical composition, matrix microstructure and free graphite characteristics (nodularity, nodule count and nodule size) are listed in the caption of each picture.

3.1. Tensile fracture surfaces

This section is concerned with the fracture surfaces of samples with different matrices tested under slow monotonic load (tension) at room temperature.

Fig. 2 illustrates a sample with a ferritic matrix; the picture with lower magnification (2a) displays an irregular topography. The higher magnification in (2b) allows observing the way in which the fracture mode advances in agreement with the main cause of fracture of the most common structural alloys, a process known as tearing and microvoid coalescence. There exists a high degree of deformation around the spheroids, and the ferritic space between nodules undergoes a substantial plastic deformation exhibiting dimples (2c). The behavior of such ductile matrix can be analyzed in the light of macrovoid coalescence, represented by the graphite nodules interacting with the microvoids present in the LTF zones and with other defects of the ferritic matrix. The internodular spaces of the ferritic matrix feature a sharp boundary or lip, due to the high degree of deformation. They are formed at the final stage of the coalescence, just before fragmentation (2d).

Fig. 3 shows ADI, a material with greater strength and lower elongation than ferritic DI, conferred by its ausferritic matrix. The deformation around graphite nodules is lower than that of the matrix previously analyzed; and the internodular zones feature dimple rupture combined with some cleavage sites, probably generated when the propagating crack cruises through LTF zones. In this case, the mechanism is mixed and governed by the characteristics of void coalescence and the LTF zones with lower strength and ductility than that of the ausferritic matrix. Probably, the mechanism combines the characteristic of microvoid coalescence through the ausferritic zones, and changes to a cleavage mode when the propagating crack reaches an LTF zone, where the presence of a carbide, for example, induces cleavage. In the literature, this mixed mechanism is referred to as quasi cleavage.

Fig. 4 illustrates the fracture surfaces corresponding to a pearlitic matrix, a microstructure with limited plastic deformation capacity, and which predominantly exhibits brittle fractures with river patterns.

At 20X and 100X (Fig. 4a and b), it is evident that the fracture surface differs from that of the ferritic and ADI matrices, resulting in a very flat surface. Nodular cavities remain practically unstrained (4c). This type of fracture consists in a crack propagating along well-defined low index crystallographic planes, known as cleavage planes. Cleavage fractures are transgranular, low-energy fractures that mainly derive from the separation of atomic bonds on low-index atomic planes. In view of the fact that cleavage occurs along well-defined crystallographic planes within each grain, cleavage fractures change directions when they cross grain or subgrain boundaries graphite nodules, LTF imperfection, etc., which explains the just mentioned river pattern observed in (4d).

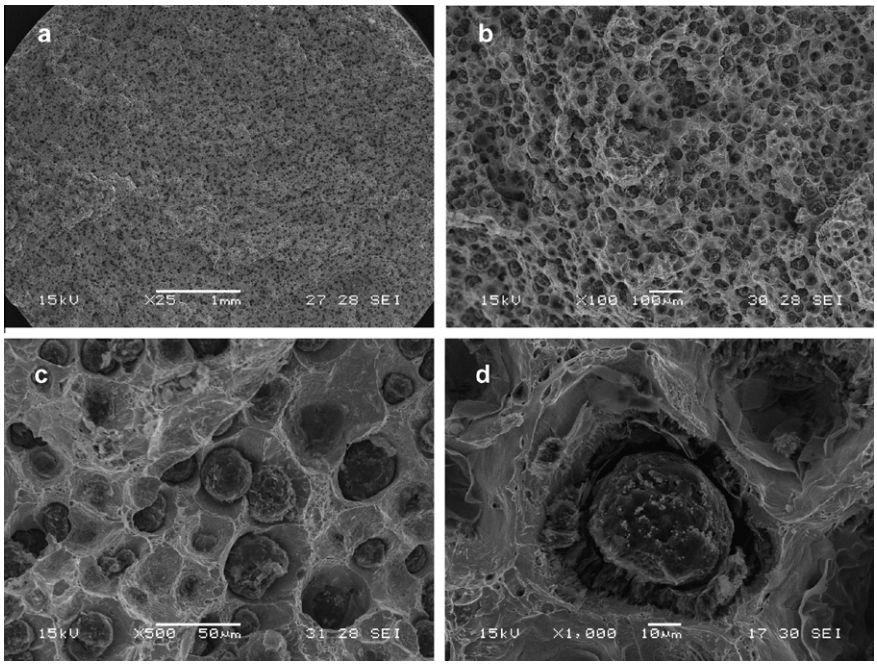

Fig. 2. Ferritic matrix tested in uniaxial tension at room temperature. Different magnifications. Chemical composition: C:3.52, Si:3.21. Mn:0.46, S:0.02, P:0.02, Mg:0.04, Cu:0.94, Ni:0.04, CE:4.48. Nodularity: 100%, nodule size: 5, nodule count: 120 nod/mm^2. UTS = 517 MPa, YS = 374 MPa, elongation% = 25.

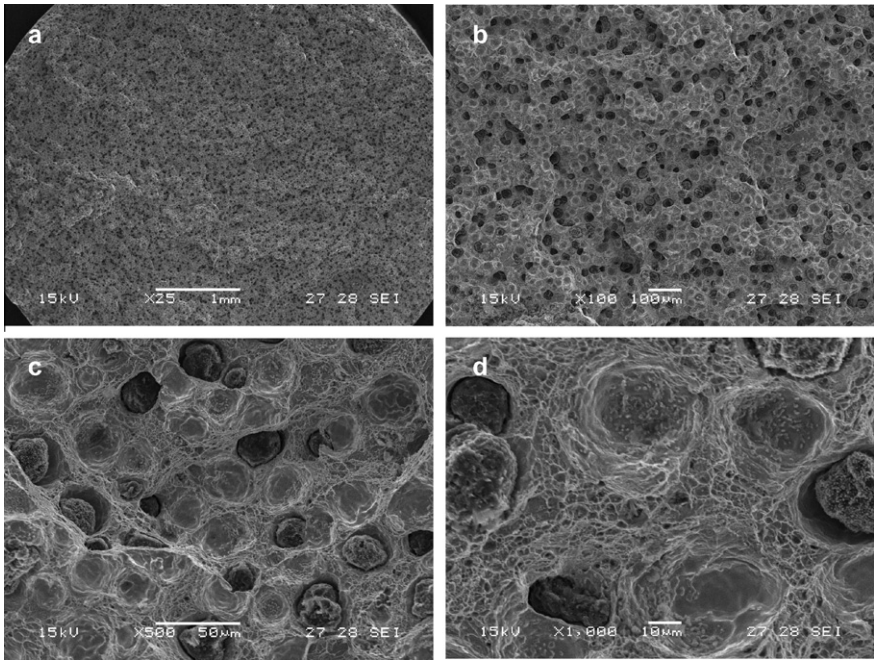

Fig. 3. ADI matrix tested in uniaxial tension at room temperature. Different magnifications. Chemical composition: C:3.52, Si:3.21. Mn:0.46, S:0.02, P:0.02, Mg:0.04, Cu:0.94, Ni:0.04, CE:4.48. Nodularity: 100%, nodule size: 5, nodule count: 120 nod/mm^2. Heat treatment: 60 min@900 °C, molten salt bath 60 min@360 °C. UTS = 1168 MPa, YS = 896 MPa, elongation% = 16.

Finally, Fig. 5 shows the fracture surfaces of martensitic ductile iron. This is a very distinctive surface where a mixed fracture mode occurs with cleavage zones and intergranular fractures. The matrix around the graphite nodules exhibits no sign of deformation. Martensite features low strain behavior, which leads to think about low deformation rate mechanisms as well as about the predominant mode of cleavage. The transgranular sites are probably induced as a favorable growing path

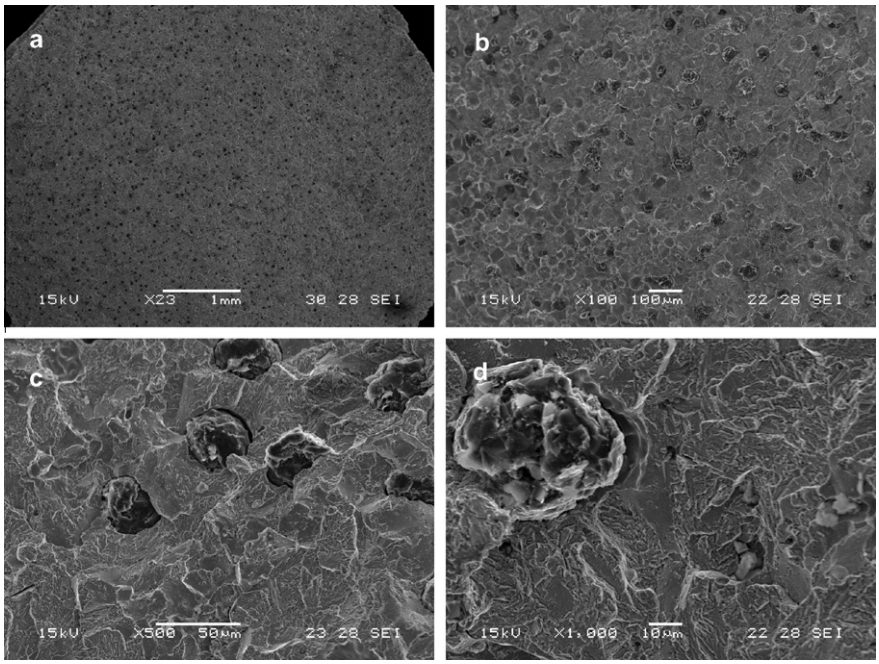

Fig. 4. Pearlitic matrix tested in uniaxial tension at room temperature. Different magnifications. Chemical composition: C:3.52, Si:3.21. Mn:0.46, S:0.02, P:0.02, Mg:0.04, Cu:0.94, Ni:0.04, CE:4.48. Nodularity: 100%, nodule size: 5, nodule count: 120 nod/mm^2. Heat treatment: 60 min@900 °C, cooled in air. UTS = 998 MPa, YS = 786 MPa, elongation% = 6.5.

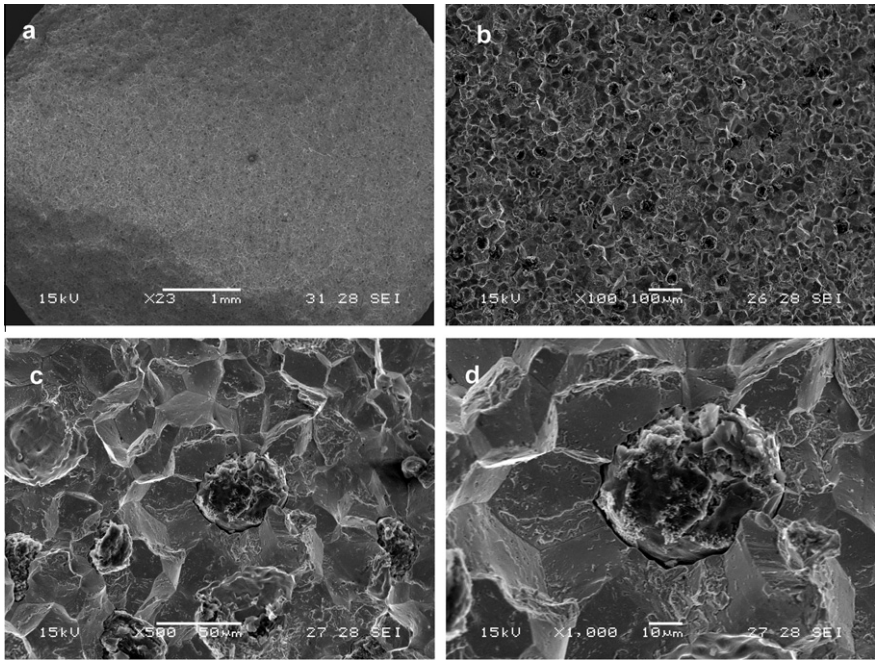

Fig. 5. Martensittic matrix tested in uniaxial tension at room temperature. Different magnifications. Chemical composition: C:3.52, Si:3.21. Mn:0.46, S:0.02, P:0.02, Mg:0.04, Cu:0.94, Ni:0.04, CE:4.48. Nodularity: 100%, nodule size: 5, nodule count: 120 nod/mm^2. Heat treatment: 60 min@900 °C, quenched in oil. UTS = 1200 MPa, elongation% = 2.

as a result of impurities segregation during quenching heat treatment, such as phosphorus and sulfur to prior austenite grains boundaries, thereby reducing the cohesive strength of the zone.

3.2. Fracture surfaces of impact tests

The fracture surfaces obtained after conducting the impact test provide new alternatives of load bearing (fast monotonic) and open the possibility of introducing the test temperature to evaluate its effect on the fracture mechanism involved.

The fracture surface of an ADI sample austempered at 360 °C and tested at 80 °C (i.e., the upper shelf zone of the transition curve) is observed in Fig. 6a and b, respectively. The fracture occurs after large plastic deformation, and is characterized by the presence of dimples and strained nodular cavities. Despite the fact that the fracture process occurs at very high speed, the plasticity mechanisms work in a similar way as when a slow monotonic load is applied.

The fracture mechanism is, again, growth and coalescence of nodular cavities and imperfections of the matrix. When the surfaces are observed at higher magnification (Fig. 6b), some dispersed isolated cleavage facets can be identified, and it is possible to conclude that the mechanism is quasi cleavage.

The general appearance does not differ significantly when samples are tested at room temperature (20 °C). Yet a more detailed observation (400X) allows identifying a larger number of cleavage facets at the internodular spaces if compared to the sample tested at 80 °C.

At low temperatures (around −40 °C (Fig. 6e), lower shelf), the fracture surfaces become flat and the cleavage facets can be observed in almost all the metallic matrix. The deformation around nodules is also negligible. The plasticity mechanisms are suppressed by the temperature effect on the dislocation movement.

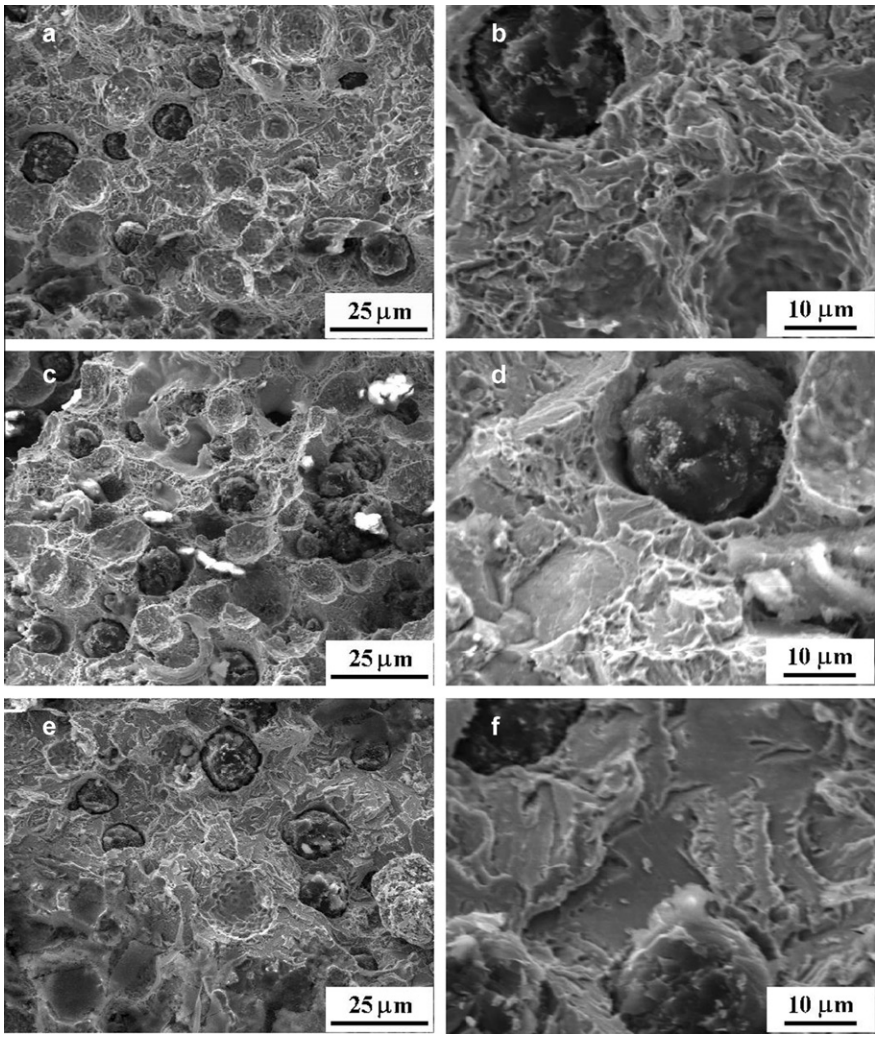

Fig. 6. ADI matrix impact tests at different temperatures. Different magnifications. Chemical composition: C:3.45, Si:2.6, Mn:0.3, S < 0.01, P:0.01, Mg:0.04, Cu:1, Ni:.5, CE:4.31. Nodularity: 100%, nodule size: 5, nodule count: 120 nod/mm^2. Heat treatment: 60 min@920 °C, Molten salt bath 1 h30 min@360 °C. UTS = 998 MPa, YS = 786 MPa, elongation% = 6.5. (a and b) Test temperature 80 °C, absorbed energy 140 J. (c and d) Test temperature 20 °C, absorbed energy 130 J. (e and f) Test temperature −40 °C, absorbed energy 100 J.

3.3. Fatigue and bending fracture surfaces

Two very well-defined zones can be observed from the resulting fragments of fracture toughness test samples in the same fracture surface. The fatigue pre-crack zone is followed by that tested with slow monotonic load in a three-point bending configuration.

The fatigue fracture surfaces analyzed in this work were generated by cyclic loading and can be considered as part of the well-known stage II of a fatigue test which follows the initiation resulting from a previously machined and sawed notch (according to the procedure detailed in ASTM E399).

Fig. 7a depicts a sample with ADI microstructure, in which the demarcation line between the fatigue (zone 1) and the bending monotonic load (zone 2) can be clearly distinguished.

At first sight, the fatigue growth zone seems to be completely flat. The fracture is characterized by rugged striations and by facets with different arrangements, sizes and micromorphologies. The matrix around the nodules has relatively opened up or stretched, and the graphite nodules show rupture signs. This fracture surface contrasts with that seen in the previous section, in which the propagation mode in monotonic fractures (tension, bending, and impact) was very ductile with considerable stretching of nodular cavities.

The pre-crack fracture surface reveals that the advancing crack cut a few nodules (note that the nodules density observed in the surface is lower than that observed in the bending growth zone). This observation comes to show that graphite nodules do not play such a strong role as they do in overload rupture processes.

Therefore, it can be concluded that the application of cyclic loads results in cracks which grow due to a mechanism that differs from that of defects growth and coalescence.

It is generally established that, during stage II, cracks tend to follow crystallographic planes, changing direction at discontinuities, such as grain boundaries, etc.

According to the literature available, two models help explain stage II striation forming fatigue propagation [8]. One is based on plastic blunting at the crack tip, though this model does not adequately predict the peak to peak and valley to valley matching of the corresponding features on fractures mating halves. The other model, which relies on a slip of the crack tip, sustains that slips cannot occur exactly at the crack tip, due to the presence of lattice or microstructural imperfections.

Stress concentration at a fatigue crack results in plastic deformation (slip) being confined to a small region at the tip of the crack while the remaining of the material is subjected to elastic strain (Fig. 8a), the crack opens on the rising tension of the load cycle by slipping on alternating slip planes. As the slip proceeds, the crack tip blunts. Yet it is re-sharpened by partial slip reversal during the declining load portion of the fatigue cycle. This leads to a compressive stress at the crack tip owing to the relaxation of residual elastic tensile stresses induced in the material uncracking during the rising load cycle (Fig. 8b). The closing crack does not re-weld, because the new slip surfaces created during the crack opening displacement are instantly oxidized, which makes complete slip reversal unlikely.

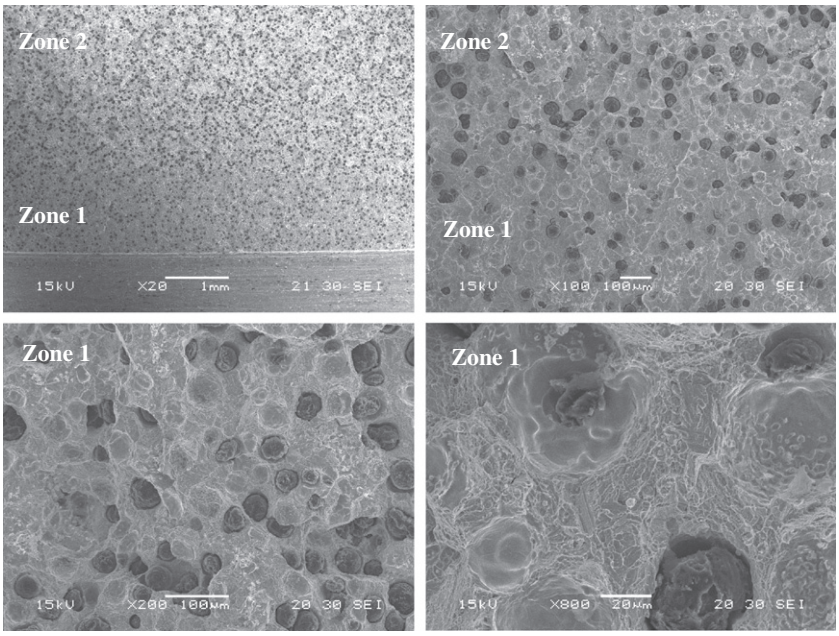

Fig. 7. Ausferritic matrix (ADI) fracture toughness test. Different magnifications. Chemical composition: C:3.52, Si:3.21. Mn:0.46, S:0.02, P:0.02, Mg:0.04, Cu:0.94, Ni:0.04, CE:4.48. Nodularity: 100%, nodule size: 5, nodule count: 120 nod/mm^2. Heat treatment: 60 min@900 °C, molten salt bath 60 min@360 °C. UTS = 1085 MPa, YS = 729 MPa, elongation% = 10, HB 357. Absorbed energy = 124 J. K_{IC} = 62 MPa m$^{1/2}$.

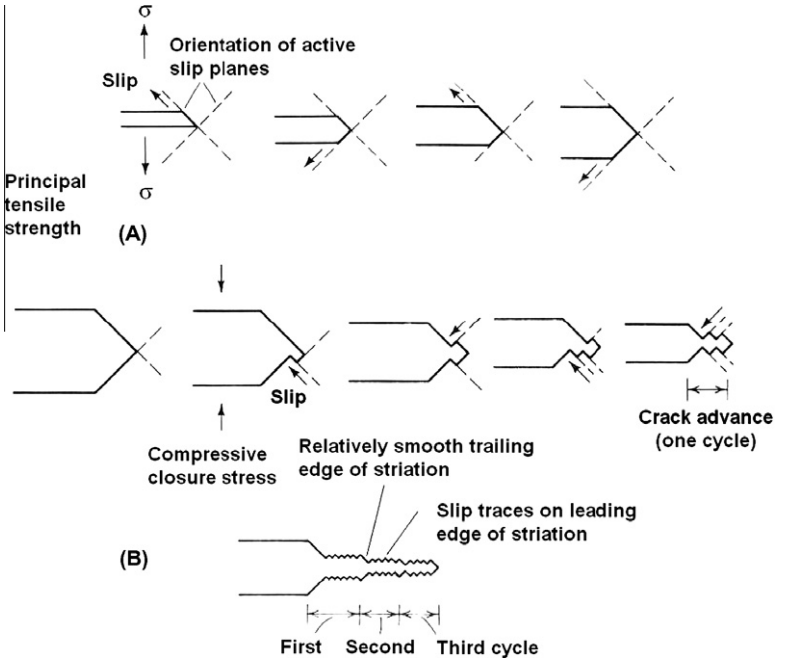

Fig. 8. Crack advance under fatigue load.

Most probably, the second model is the one that better explains the mechanism involved in ductile iron crack propagation.

This mechanism, applied to the growing cracks on ADI, displays a mixture of striations resulting from the advance of a propagating crack over the ferrite and fractured austenite needles.

When crack length was increased, i.e., with a higher stress intensity factor, the changes detected in the overall morphology of the fracture surfaces were practically negligible.

The zone corresponding to the fracture generated by the three-point bending test (zone 2) features similar characteristics to those described in samples tested with a slow monotonic load. Besides, the fracture mechanism can be associated to voids growth and coalescence; although, in this case, the deformation of the nodular cavities is oval shaped if compared to those fragmented by uniaxial stress.

The fracture surfaces of the ferritic matrix are shown in Fig. 9. Striations are noticed in all cases. Said striations have a step-like shape rather than macroscopic waviness or undulations. The analysis above conducted for ADI can also be extended to the ferritic matrix; yet the fracture is not as flat as in the case of ADI. The nodules density observed in the surface is greater.

The greater plastic deformation capacity of ferrite plays a key part in the propagation process in this case.

A detail of the rugged surfaces is illustrated in the pictures of Fig. 10.

A sort of macrotongues (depicted by arrows) aligned with the propagation direction are observed for both matrices (Fig. 11), being more pronounced in the case of the ferritic matrix.

The propagation mode in monotonic fractures (bending) is very ductile with considerable stretching of nodule bearing cavities. The deformation of the nodular cavities exhibits, again, an oval shape with the longest axis of the ellipse in the direction of the crack propagation. Fig. 12 displays a comparison of nodular equiaxed and oval strained for both matrices under study.

The propagation of cracks by means of cyclic loads enables to interrupt the test and analyze the previously polished lateral surface of the sample at different times; also to observe the microstructural zone chosen by the propagating crack. The metallographic analyses, observing the sample from one side, show that the fracture path of entirely ferritic matrices exhibits transgranular propagation. (Fig. 13a and b). The zones with greater plastic deformation are evident in the fracture path and in its vicinity. Branching advance of the main crack can also be detected.

Fig. 14 illustrates the lateral crack advance examination of an ADI sample. A straight crack advance in the direction of the ausferrite needles can be observed.

Especially in steels, fatigue striations often bow out in the direction of crack propagation and generally tend to align perpendicular to the principal crack propagation direction. However, variations of local stresses and microstructure can change the orientation of the plane of fracture and alter the direction of the striation alignment.

Large second phase particles, such as nodules and inclusions in the metallic matrix (LTF), can change the local crack growth rate and result in fatigue striation spacing. When a fatigue crack approaches a nodule, it is briefly retarded. As a mat-

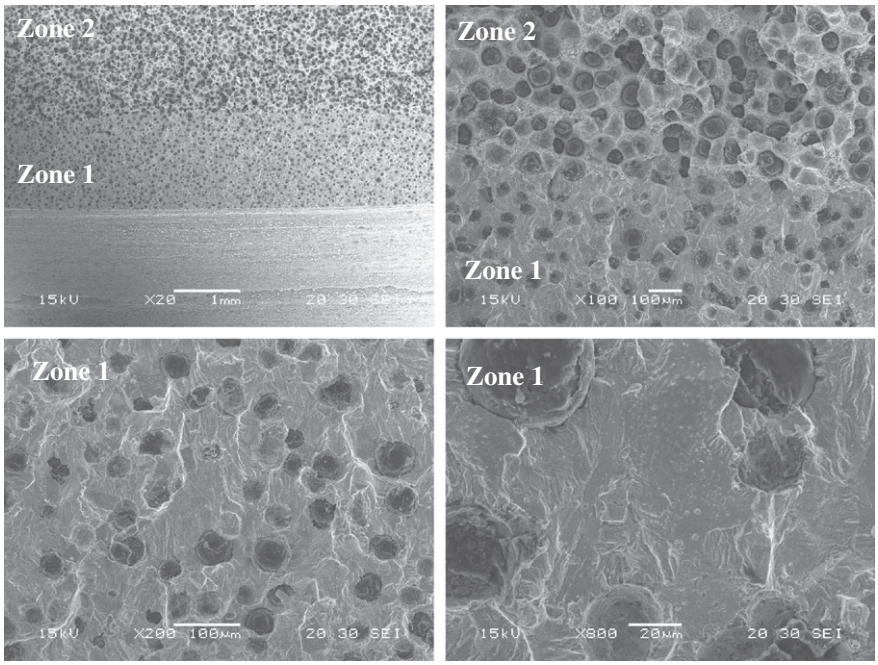

Fig. 9. Ferritic matrix DI fracture toughness test. Different magnifications. Chemical composition: C:3.52, Si:3.21. Mn:0.46, S:0.02, P:0.02, Mg:0.04, Cu:0.94, Ni:0.04, CE:4.48. Nodularity: 100%, nodule size: 5, nodule count: 120 nod/mm^2. Heat treatment: fertilizing. UTS = 455 MPa, YS = 332 MPa, elongation% = 26, HB173. K_{IC} = 43 MPa m$^{1/2}$.

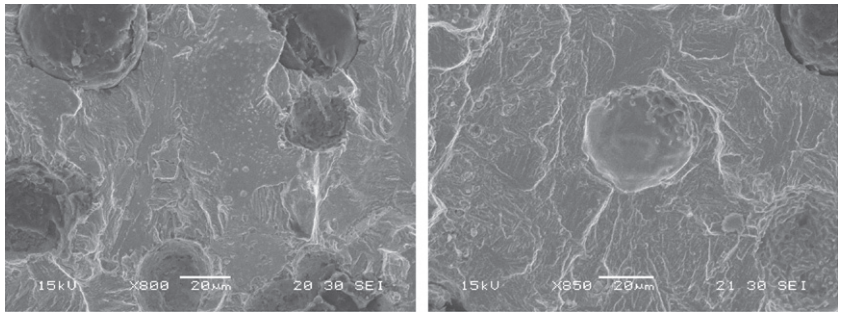

Fig. 10. Detail of striations on both matrices.

ter of fact, the crack finds a microblunt notch at the end of the crack, and depending on the matrix type it can be a suitable site to switch to the cleavage mode, thereby accelerating the process. In both cases, however, the crack growth rate is changed only in the immediate vicinity of the particle and therefore does not significantly affect the total crack growth rate.

3.4. Special case of fracture on austempered ductile iron

3.4.1. Environmentally assisted embrittlement

Austempered ductile iron is known to suffer a noticeable embrittlement when its surface is in contact with liquids during slow monotonic load tensile testing [9,10]. Reductions of about 25% in UTS and 75% of elongation were measured when samples were tested with their surface in contact with water, the most deleterious of all the tested fluids (alcohol, organic reagents, etc.) [11].

Masud et al. [12] explored the relationship existing between the flat fracture regions on the fracture surface of tensile testing samples, and the fracture initiation site. In an attempt to localize the initiation of the fracture, the tensile sample surface was put in contact with water only at a very small location, by using a (cotton swab) previously wet with water. This was done during the test, at a constant stress level higher than the tensile strength reached in contact with water, but lower than the dry ultimate tensile strength.

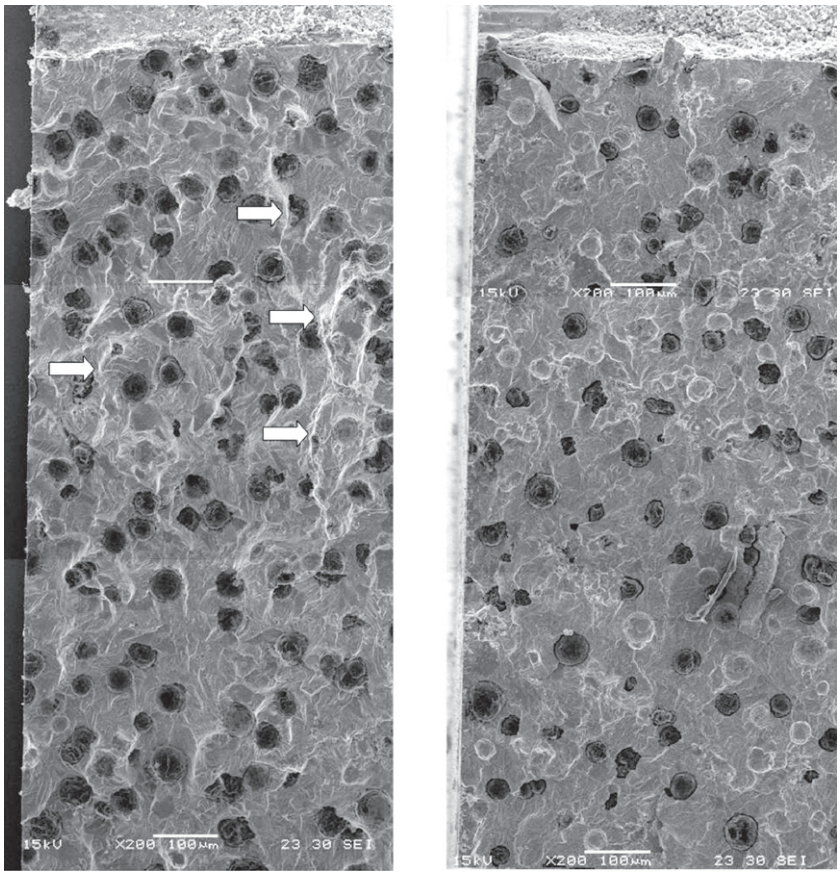

Fig. 11. Macrotongues aligned with the propagation direction.

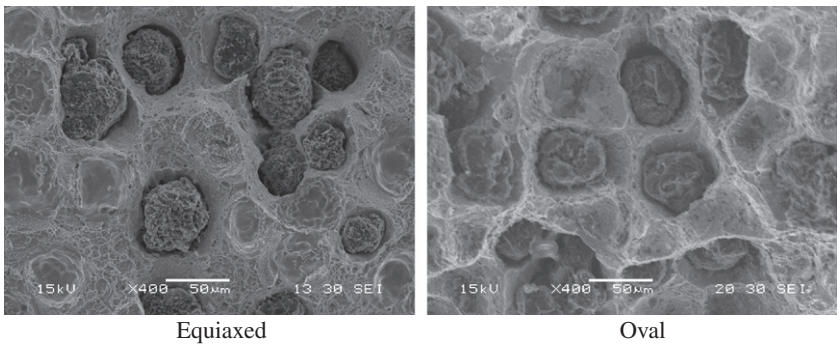

Fig. 12. Comparison of equiaxed and oval strained nodular cavities.

Under this stress condition, the contact of the wet cotton slab on a flat surface of a cylindrical tensile specimen caused instantaneous fracture.

Fig. 15a shows different zones of the fracture surface obtained. The arrow points to the site where the sample was touched and the line surrounds a nearly round, bright and flat fracture area resulting from the (cotton swab) point of contact. The examination of the fracture surface, performed by scanning electron microscopy, showed that the fracture mechanism that characterizes the flat region is cleavage, as shown in Fig. 15b.

Cracks initiation and propagation occur immediately, with the fracture propagating through the entire test specimen. Crack velocity or fracture propagation was estimated at 10–100 cm/s.

The appearance of the remaining fracture surface (Fig. 15c and d) is similar to that described for a normal overload fracture in ADI, already described as a quasi cleavage fracture in Section 3.1 (Fig. 3).

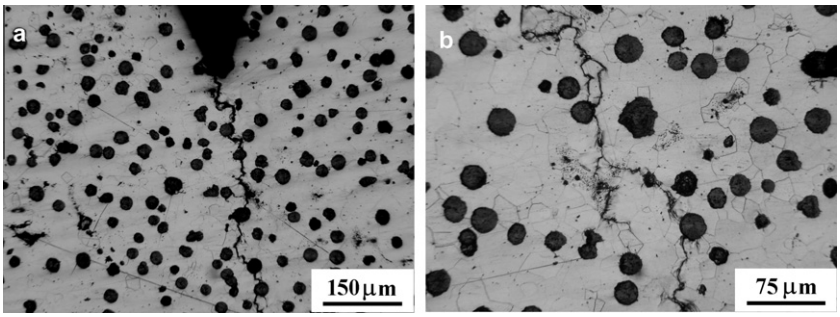

Fig. 13. Lateral surface of a fatigue cracked ferritic DI sample.

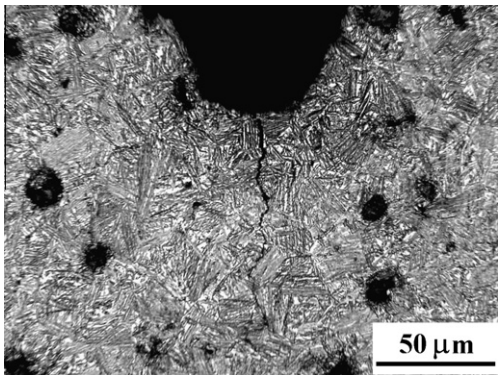

Fig. 14. Lateral surface of a fatigue cracked ADI sample.

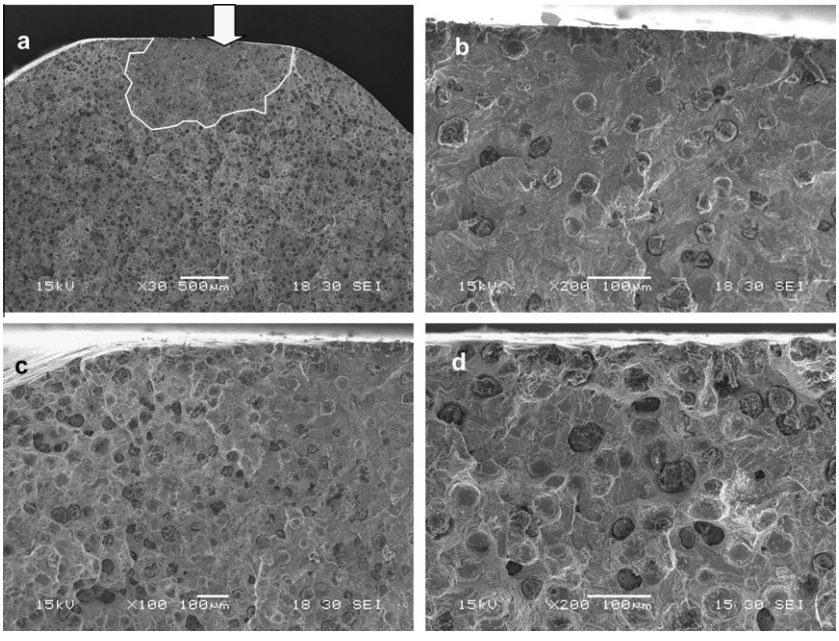

Fig. 15. Aspect of a sample tested in contact with water at a localized point.

Based on the literature available and given the similarities with liquid metal embrittlement (LME) [13], the authors propose that the fracture of ductile iron in contact with water is as follows: upon stressing ADI at a certain level above its yield strength, it develops cracks at the LTF regions, as shown by Laine [14]. When this takes place in contact with water or other

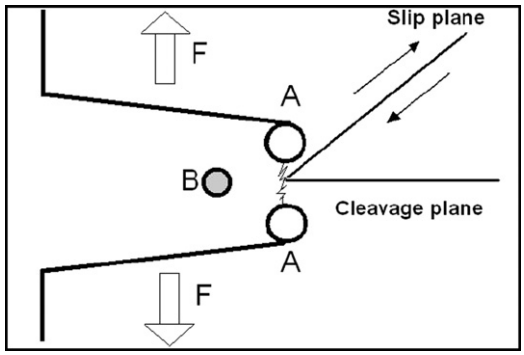

Fig. 16. Schematic representation of the weakening of A–A atom bonds at a surface crack tip as a result of the interaction with an atom or molecule B supplied by the surrounding liquid.

liquids, the liquid penetrates the crack, the A–A atomic bonds at the crack tip are weakened by the chemisorption of an atom or molecule B, as schematically shown in Fig. 16.

The chemisorption process presumably takes place spontaneously or only after the A–A bonds have been strained to some critical value. In any event, electronic rearrangement takes place because of adsorption, weakening the bonds at the crack tip. When the applied remote stress is increased so that local stress at the crack tip exceeds the reduced breaking strength of A–A bonds, the crack becomes unstable and grows rapidly. The crack grows initially in a brittle manner, by cleavage, but changes to a ductile mechanism, as it grows far from the fracture initiation site. Taking into account the load conditions under tensile testing, the stress levels, and the sample dimensions, and assuming a semielliptical surface defect and a K_{IC} value of 90 MPa $m^{1/2}$, the size of the critical defect can be estimated to be 0.8 mm. This would indicate that if the presence of water activates the rapid growth of a crack, and such crack extends beyond the critical defect size, then, even when the fracture mode changes to a higher energy consuming mechanism, the remaining ligament will not be able to stop fracture, and the sample will collapse. The size of the cleavage fracture surface observed in tensile specimens fractured in contact with water, as shown in Fig. 15, is usually nearly 1.5 mm. This size is greater than the critical defect size, supporting the proposed mechanism.

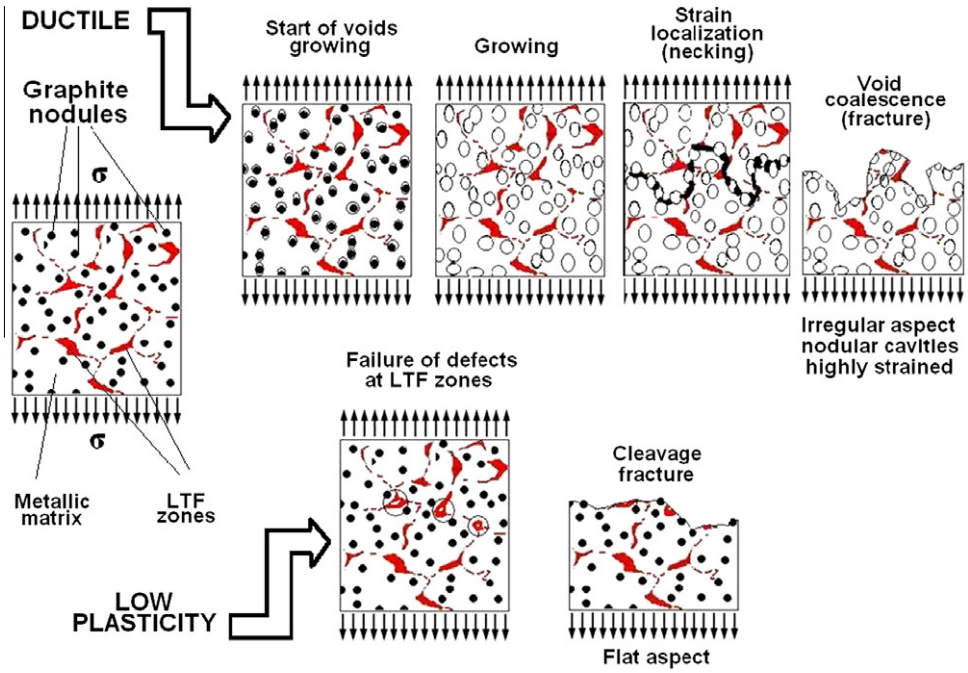

Fig. 17. Proposed model for ductile and low plasticity fracture with samples tested at slow monotonic load (tension).

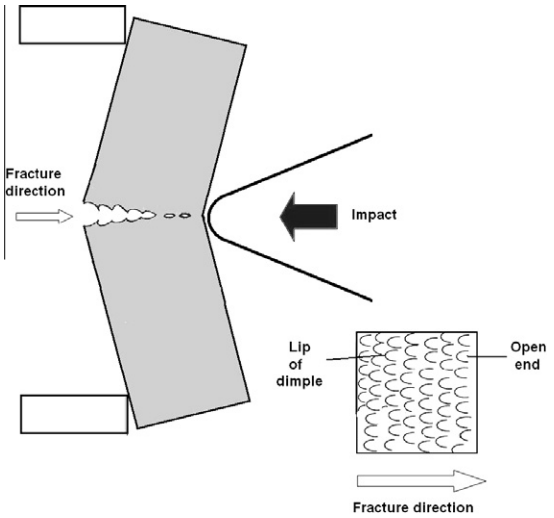

Fig. 18. Sketch of dimple shape formed under tear loading conditions.

4. Remarks and final conclusions

- When slow monotonic loading is applied to ferritic and ausferritic matrices, the operative mode at ambient temperatures is ductile tearing with microvoid coalescence. Dimple fracture in the metallic matrix exhibits numerous cuplike depressions which result directly from microvoid coalescence. The size and distribution of the dimples is governed by the size and distribution of the nucleated voids. For instance, when the voids are few and widely spaced, they grow to a large size before coalescing and the result is a fracture surface that contains large dimples. Cleavage fracture tends to initiate at the inclusions around the eutectic cell boundary (LTF) rather than at the graphite nodule–matrix interface.

The propagating crack will cut through any other non-spheroidal form of graphite that may be present. A good example is the fracture surface of the pearlitic matrix tested at tensile slow monotonic load.

A proposed model for both fracture modes with slow monotonic load (tension) is sketched in Fig. 17.

- In matrices with higher strength and toughness the spherical discontinuities present in the material feature a lower deformation percentage and hence the defects, carbides and martensite (induced by strain transformation of retained austenite) present in the LTF have a key role in the fracture mechanism. This is the case of ADI with an ausferritic matrix.

The appearance of the fracture surface is quasi cleavage, composed by zones with ductile fractures (crack advance over ausferrite) and facets of cleavage (crack advancing over brittle LTF).

- Fracture surfaces generated by tear loading conditions exhibit elongated dimples into the metallic matrix, with one of its axis longer than the other one and with one of its ends open, i.e., the dimple is not completely surrounded by a rim. Fig. 18 sketches this situation, which is observed in Fig. 6b. The elongated dimples on both fracture surfaces are oriented in the same direction and the closed ends point to the fracture origin. This characteristic of tear dimples can be used to establish the fracture propagation direction.
- Pearlitic matrices, a fine alternating lamellae mixture of ferrite and cementite, offer a preferential path for propagation in the second component. The result is a typical cleavage surface.
- Martensitic matrices present some sites with cleavage and transgranular fracture zones probably due to impurities segregation during the applied thermal cycles. Elements like phosphorus and sulfur, placed in prior austenite grains boundaries, reduce the cohesive strength of the zone.
- Dimple shape is governed by the state of stress within the material as the microvoids grow and coalesce. Fracture under uniaxial tensile load conditions result in the formation of essentially equiaxed dimples bounded by a lip or rim.
- Depending on the microstructure and plasticity of the material the dimples can either exhibit a very deep conical shape or be quite shallow.
- When the temperature or load application mode allows dislocation displacements, initial deformations concentrate in the bounds of graphite nodules, these cavities acting as stress concentrators. Cavities growth ends with their coalescence, giving a fibrous aspect to the fracture surface characterized by the presence of a large number of dimples. This behavior can

be ascribed to ferritic matrices with certain differences, depending on the nature of the load, temperature, etc. As test temperature drops below ambient, the fracture mode at a slow monotonic load rate undergoes a gradual ductile to brittle transition.

Acknowledgements

The author wish to thank the financial support granted by CONICET, FONCYT and the Universidad Nacional de Mar del Plata.

References

[1] QIT Fer et titane Inc. Ductile iron data for design engineers. Montreal, Quebec; 1990.
[2] Rivera G, Boeri R, Sikora J. Int J Cast Metals Res 1995;8(1):1–5.
[3] Rivera G, Boeri R, Sikora J. Int J Cast Metals Res 1999;11:533–8.
[4] Boeri R, Weingberg F. Int J Cast Metals 1993;6:153–8.
[5] Anderson TL. Fracture mechanics; fundamentals and applications. CRC Ed.; 1995.
[6] Barsom JM, Rolfe ST. Fracture and fatigue control in structures, application of fracture mechanics. 2nd ed. Englewood Cliffs, New Jersey 07632 USA: Prentice-Hall; 1987.
[7] Broek D. Elementary engineering fracture mechanics. 4th ed. 101 Philip Dr., Norwell, MA 02061 USA: Kluwer Academic Publishers; 1991.
[8] ASM metals handbook. 9th ed., vol. 12. Fractography; 1987.
[9] Shibutani S, Komatsu S, Tanaka Y. Embrittlement of austempered spheroidal graphite cast iron. Int J Cast Metals Res 1999;11:579–85.
[10] Martínez RA, Boeri R, Sikora JA. Embrittlement of ADI caused by contact with water and other liquids. Int J Cast Metals Rev 2000;13:9–15.
[11] Martínez RA, Simison SN, Boeri RE. Environmentally assisted embrittlement of ADI by contact with liquids. Int J Cast Metals Rev 2003;16(1–3):251–6.
[12] Masud L, Martínez RA, Simison S, Boeri RE. Embrittlement of austempered ductile iron on contact with water – testing under applied potential. J Mater Sci 2003;38:2971–7.
[13] Metals handbook. Corrosion, 9th ed., vol. 13. ASM International.
[14] Laine B. M. E. Thesis – INSA (Institut National des Sciences Apliquées)–Lyon–FRANCE "Estudio del fenómeno de fragilización de fundiciones esferoidales austemperizadas". Presented at Materials Department – Universidad Nacional de Mar del Plata; 2001.